First-principles calculations of the thermodynamic mixing properties of arsenic incorporation into pyrite and marcasite

Martin Reich [a,b,*], Udo Becker [a]

[a] *Department of Geological Sciences, University of Michigan, 2534 C.C. Little Building, 1100 North University Ann Arbor, Michigan 48109-1005, USA*

[b] *Departamento de Geología, Facultad de Ciencias Físicas y Matemáticas, Universidad de Chile, Santiago, Chile*

Abstract

The thermodynamic mixing properties of As into pyrite and marcasite have been investigated using first-principles and Monte Carlo calculations in order to understand the incorporation of this important metalloid into solid solution. Using quantum-mechanical methods to account for spin and electron transfer processes typical of sulfide minerals, the total energies of different As–S configurations were calculated at the atomic scale, and the resulting As–S interactions were incorporated into Monte Carlo simulations. Enthalpies, configurational entropies and Gibbs free energies of mixing show that two-phase mixtures of FeS_2 (pyrite or marcasite) and FeAsS (arsenopyrite) are energetically more favorable than the solid solution $Fe(S,As)_2$ (arsenian pyrite or marcasite) for a wide range of geologically relevant temperatures. Although miscibility gaps dominate both solid solution series, the solubility of As is favored for $X_{As}<0.05$ in iron disulfides. Consequently, pyrite and marcasite can host up to ~6 wt.% of As in solid solution before unmixing into (pyrite or marcasite)+arsenopyrite. This finding is in agreement with previously published HRTEM observations of As-rich pyrites (>6 wt.% As) that document the presence of randomly distributed domains of pyrite+arsenopyrite at the nanoscale. According to the calculations, stable and metastable varieties of arsenian pyrite and marcasite are predicted to occur at low ($X_{As}<0.05$) and high ($X_{As}>0.05$) As bulk compositions, respectively.

Keywords: Arsenian pyrite; Solid solution; First-principles calculations; Monte Carlo simulations

1. Introduction

Under reducing conditions, iron sulfides such as pyrite/marcasite polymorphs (FeS_2) and arsenopyrite (FeAsS), and arsenides such as löllingite ($FeAs_2$) are major hosts for arsenic in geologic environments (Savage et al., 2000; Sidle et al., 2001; Utsunomiya et al., 2003). When exposed to oxidizing conditions, these minerals release significant amounts of this toxic metalloid into natural waters and soils, in some cases producing serious arsenic poisoning as observed, e.g., in Bangladesh (Anawar et al., 2003). In addition, when precipitated from hydrothermal solutions, arsenic-bearing iron sulfides such as arsenian pyrite/marcasite and arsenopyrite incorporate significant amounts of trace metals (thousands of ppm), especially gold (Palenik et al., 2004; Reich et al., 2005, and references therein).

Although the chemistry, speciation, and thermodynamic stability of As in aqueous solutions have been

* Corresponding author. Department of Geological Sciences, University of Michigan, 2534 C.C. Little Building, 1100 North University Ann Arbor, Michigan 48109-1005, USA. Tel.: +1 734 763 9368; fax: +1 734 763 4690.

E-mail address: mreichm@umich.edu (M. Reich).

extensively studied, the solid solution of As in iron sulfide minerals is still not well understood. Natural arsenian pyrite and marcasite ($Fe(S,As)_2$) formed at temperatures below about 300 °C can incorporate up to ~19 wt.% As (Sha, 1993; Simon et al., 1999b; Cline, 2001; Reich et al., 2003), and experimental studies at higher temperatures (300–600 °C) have reported As solubilities of up to 9.3 wt.% and 16.5 wt.% As in pyrite and marcasite, respectively (Clark, 1960; Kretschmar and Scott, 1976; Fleet and Mumin, 1997). Although these results define a general compositional range for As incorporation into pyrite and marcasite, its maximum solubility remains unconstrained. Synchrotron XANES/EXAFS studies have documented that As replaces S as As^{-1} in arsenian pyrite and arsenopyrite (Simon et al., 1999a; Cabri et al., 2000; Savage et al., 2000), and a widespread persistence of metastable solid solution for As between the FeS_2–FeAsS join in the Fe–As–S system has been reported (Fleet et al., 1989; Fleet and Mumin, 1997). Although the experimental results suggest a complete solid solution of As between pyrite/marcasite and arsenopyrite compositions, TEM observations of stacking faults (Fleet et al., 1989; Simon et al., 1999a) and nanoscale domains of pyrite and arsenopyrite (Palenik et al., 2004) in As-rich pyrite samples indicate a miscibility gap between FeS_2 and FeAsS end-members. On the other hand, HRTEM and XANES/EXAFS data by Savage et al. (2000) suggest clustering of arsenic atoms in the solid solution instead of nanoscale heterogeneity.

The thermodynamic stability of As-bearing iron sulfides has not been determined experimentally at temperatures below ~300 °C. Under these conditions, equilibrium is difficult to obtain in laboratory synthesis because nucleation of pyrite and marcasite does not proceed at a significant rate at low temperatures (Schoonen and Barnes, 1991a,b,c). Hence, with the exception of early studies on the phase equilibria of the Fe–As–S system (Clark, 1960; Barton, 1969; Kretschmar and Scott, 1976), and more recent studies on arsenopyrite stability in crustal fluids at high temperature (>300 °C) (Pokrovski et al., 2002), thermodynamic data are lacking for arsenian pyrite and arsenian marcasite, two major sources of As. This lack of information, added to the absence of activity models for the incorporation of As into solid solution, has limited our understanding of the conditions that govern formation and decomposition of these As-bearing sulfides in natural environments.

In this study, the thermodynamic mixing properties of arsenian marcasite and pyrite solid solutions were calculated using first-principles (ab initio) methods to evaluate the stability (or metastability) of arsenian iron disulfides in nature. The energetics of As incorporation into solid solution was calculated within the framework of the marcasite, pyrite, arsenopyrite and löllingite structures. In order to derive the excess enthalpy of mixing (ΔH_{excess}) of the solid solutions, these results were incorporated into Monte Carlo simulations, and subsequently, the Gibbs free energy (ΔG_{excess}) and entropy (ΔS_{excess}) of mixing were calculated using a Bogoliubov integration scheme. Based on the thermodynamic data at equilibrium, T–X_{As} phase diagrams for the solid solution of As into marcasite and pyrite are presented and simulation results compared with available experimental and analytical data.

2. Computational methods

The computational approach used in this study to calculate the thermodynamic properties of solid solutions is illustrated by a three-step process shown in Fig. 1, and explained in detail in the following sections. As a first approximation, the central component of the simulation is based on the fact that the energy of a solid solution can be expressed in terms of individual bonds (Bosenick et al., 2001; Dove, 2001). The first step needed to obtain the thermodynamic properties of the As–S solid solutions in the Fe–As–S system is to calculate, using atomistic simulations, the total energy for a number of different configurations of As and S anions in marcasite–arsenopyrite–löllingite structure series and in the pyrite–$FeAsS_{pyr}$–$FeAs_{2,pyr}$ series (step A). Here, pyrite–$FeAsS_{pyr}$–$FeAs_{2,pyr}$ stands for successively incorporating more and more As into the isometric structure of pyrite. Even though $FeAsS_{pyr}$ and $FeAs_{2,pyr}$ are not thermodynamically stable with respect to arsenopyrite and löllingite, respectively, their calculation is instructive to show why at mole fractions $X_{As}>0.05$, only

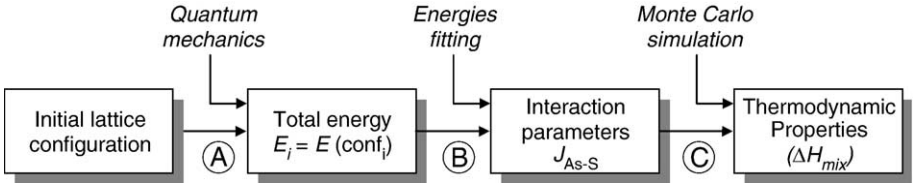

Fig. 1. Flowchart illustrating the three-step process used for the calculation of thermodynamic properties of As–S solid solution in iron disulfides.

the monoclinic and orthorhombic structure types are thermodynamically stable. Considering the fact that As substitutes for S in iron sulfide minerals (Simon et al., 1999a; Cabri et al., 2000; Savage et al., 2000; Reich et al., 2005), any As–S substitution or rearrangement of the structural relationship of As and S in the lattice is associated with a change in total energy ΔE. Subsequently, anion–anion interaction parameters (As–S, S–S and As–As) for all possible pairs of exchangeable sites are derived to closely fit all energies from the quantum-mechanical runs (step B). The excess enthalpy of mixing (ΔH_{excess}) can be calculated by using the interaction parameters in combination with Monte Carlo simulations (step C), that evaluate the energy of millions of possible configurations as a function of temperature and composition (see Bosenick et al., 2000; Becker et al., 2000; Dove, 2001; Becker and Pollok, 2002). In addition, we calculate the excess entropy and free energy of mixing (ΔS_{excess}, ΔG_{excess}) using a post-Monte Carlo Bogoliubov integration scheme (Yeomans, 1992).

2.1. Ab initio total-energy calculations

In order to calculate the lattice energy variations associated with As–S substitutions in the Fe–As–S system, the isostructural series marcasite–arsenopyrite–löllingite (FeS_2–$FeAsS$–$FeAs_2$) was selected as the structural framework for computations. Additionally, the As–S substitution in pyrite was treated separately within the pyrite framework ($Pa3$), a NaCl-like structure (the Cl atoms are replaced by disulphide groups) where the slightly distorted Fe octahedra only share corners (Fig. 2b). In contrast, in the structures of marcasite ($Pnnm$), arsenopyrite ($P2_1/c$) and löllingite ($Pnnm$), Fe octahedra share edges lying in the (001) plane of the marcasite orthorhombic cell (Fig. 2a). A detailed description and comparison of the pyrite–marcasite–arsenopyrite–löllingite structures can be found in Aylmore (1995).

In general, two methodologies can be applied to calculate the total lattice energy: (i) empirical force-field calculations and (ii) ab initio, quantum-mechanical calculations. The first method, in which the lattice energy of each configuration is obtained from a set of empirically parameterized long- and short-range potentials, is computationally efficient for large systems (tens to thousands of atoms). It is widely used with some degree of confidence to predict crystal structures and their properties, although there may not be the same confidence in predicting absolute defect energies (Heine, 1998). Unlike empirical force field methods, quantum-mechanical energies are calculated from first-principles by means of solving the Schrödinger equation ($\boldsymbol{H\Psi = E\Psi}$) for a many electrons system through a series of approximations. Although this approach is computationally more intensive and restricted to small unit cells (on the order of tens of atoms), the calculated total energies are not dependent on empirically derived parameters.

In this study, the total energy of each configuration was calculated using the quantum-mechanical (ab initio) approach. This method was chosen because some electron transfer is involved when S is replaced by As in the structure such that the interaction of As and S is predominantly covalent with varying degrees of ionicity. In addition, odd numbers of As require the

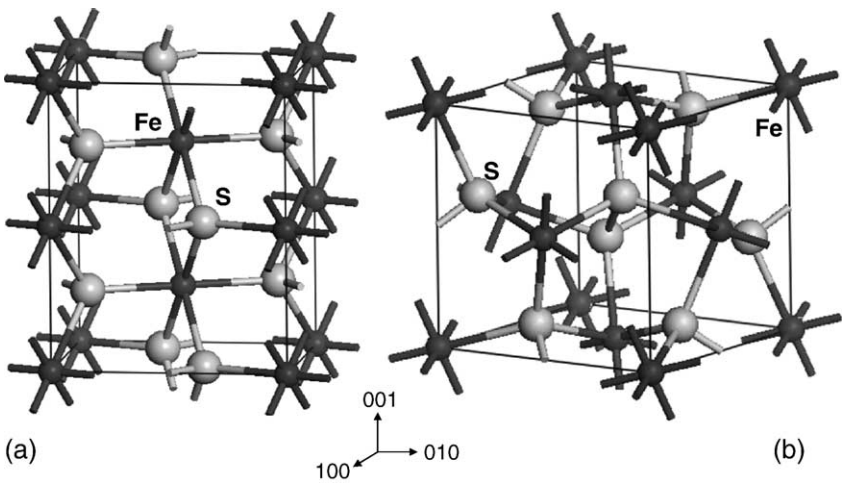

Fig. 2. (a) Atomic models for marcasite ($1 \times 1 \times 2$)-superlattice and (b) conventional pyrite lattice ($1 \times 1 \times 1$), used to calculate total lattice energies for different As–S mixtures (As substitutes S sites). Fe and S atoms are dark-gray and light-gray, respectively.

simulation of unpaired spins which cannot be captured using empirical force fields. The computational method is based on density functional theory (DFT, Hohenberg and Kohn, 1964), using plane waves as basis functions for the simulation of the wavefunctions and ultrasoft pseudopotentials to approximate the role of the core electrons (Payne et al., 1992). For these calculations, we chose $1 \times 1 \times 1$ cells for pyrite and arsenopyrite and $1 \times 1 \times 2$ supercells for marcasite and löllingite, each containing 8 exchangeable anion sites for As–S substitution. Full geometry optimization of 40 random configurations for each solid solution series (marcasite and pyrite structural frameworks) was performed using the ab initio code CASTEP (Segall et al., 2002) incorporated in the Cerius^2 software package. The Perdew–Whang generalized gradient scheme (GGA/GGS, Perdew and Wang, 1992) was used along with ultrasoft pseudopotentials (Vanderbilt, 1990). All the calculations were performed at 0 K and zero-pressure conditions for the primitive unit cell ($P1$, no symmetry restrictions) using an energy cut-off (E_{cut}) of 340.00 eV and a $2 \times 2 \times 2$ k-point grid for which convergence of the crystal structure and energy was achieved. Using these computational parameters, a good agreement was found between experimental and calculated cell parameters values for each structure (Table 1).

Table 1
Experimental and calculated (CASTEP) lattice parameters for pyrite, marcasite, arsenopyrite and löllingite

	a (Å)	b (Å)	c (Å)
Pyrite (FeS_2)			
Experimental[a]	5.42	5.42	5.42
Calculated	5.37	5.37	5.37
Deviation (%)	0.92	0.92	0.92
Marcasite (FeS_2)			
Experimental[b]	4.44	5.41	3.38
Calculated	4.40	5.37	3.37
Deviation (%)	0.90	0.74	0.30
Arsenopyrite (FeAsS)			
Experimental[c]	5.74	5.67	5.78
Calculated	5.66	5.58	5.69
Deviation (%)	1.39	1.59	1.56
Löllingite ($FeAs_2$)			
Experimental[d]	5.30	5.98	2.88
Calculated	5.28	5.95	2.86
Deviation (%)	0.38	0.50	0.69

[a] Bayliss (1977).
[b] Buerger (1931).
[c] Morimoto and Clark (1961).
[d] Fan et al. (1972).

2.2. Calculation of anion–anion interaction parameters

In general, the energy of mixing of As anions into $Fe(S,As)_2$ solid solution can be expressed by the model Hamiltonian (Eq. (1)), taking into account separate interactions for As and S ordering anions:

$$E = E_0 + \sum_i \left(n^i_{\mathrm{As-S}} E^i_{\mathrm{As-S}} + n^i_{\mathrm{S-S}} E^i_{\mathrm{S-S}} + n^i_{\mathrm{As-As}} E^i_{\mathrm{As-As}} \right) \tag{1}$$

where n_{XY} indicate the number of i-type interactions between anions X and Y, E_{XY} represents the energy contribution of that particular interaction to the total energy of the solid solution, and E_0 is a composition-dependent energy constant. Since we are interested in excess properties, the separate energy terms in Eq. (1) can be combined into exchange parameters J, which indicates the energy associated with the sole exchange between As and S (Eq. (2)):

$$J^i_{\mathrm{As-S}} = E^i_{\mathrm{As-S}} - \frac{1}{2}\left(E^i_{\mathrm{S-S}} + E^i_{\mathrm{As-As}} \right). \tag{2}$$

In consequence, by fitting the Hamiltonian to a number of previously calculated energies for different anion configurations, the interaction parameters J can be obtained. Thus, each interaction parameter represents the energy associated with the formation of an As–S pair for a given interaction i. Even though the exchange parameters J are defined based on anion–anion interactions, cation–anion interactions such as Fe–As or Fe–S are implicitly included, as the quantum-mechanical total energies were calculated for the full crystal lattice. Since the J formalism simulates these total energy values, all interactions within the lattice are implicitly included, not just anion–anion interactions.

The As–S interaction parameters ($J_{\mathrm{As-S}}$) were found by fitting the CASTEP energies E_i to different interactions $n_{\mathrm{As-S}}$, according to Eq. (3):

$$E^i_{\mathrm{CASTEP}} = E_{\mathrm{XAs}} + \sum_{i,j} \left(n^{i,j}_{\mathrm{As-S}} J^{i,j}_{\mathrm{As-S}} \right). \tag{3}$$

The best fit of the Hamiltonian was found for five types of As–S interactions: nearest-neighbors (1), third nearest-neighbors (3) and fourth, fifth and sixth nearest neighbors (4, 5 and 6, respectively). Second nearest interactions are omitted because the number of interactions within the anion dimer equals the number of second nearest-neighbors in all configurations. Thus, the matrix elements for the derivation of nearest and second nearest-neighbors interactions would be linearly dependent. The calculated Js (exchange parameters)

and E_{XAs} (composition-dependent terms) are presented in Table 2, along with r-square values indicating goodness of fit.

2.3. Monte Carlo simulation: determination of thermodynamic properties

After fitting the interactions n_i to the calculated quantum-mechanical energies E_i, the resulting interaction parameters J_i can be used to calculate the lattice energies for millions of different anion configurations. When these data are incorporated into a Monte Carlo simulation, the enthalpy of mixing of arsenian marcasite and pyrite series solid solutions is obtained. Each random switching of positions between As and S in a starting configuration (with lattice energy E) has an associated change in energy ΔE after the swap. If the final energy $E+\Delta E$ is negative, the swap is accepted with probability one. If the change in energy is positive, the swap is accepted with a probability P assigned by the Boltzmann's distribution:

$$P(E \rightarrow E + \Delta E) = \frac{1}{\exp(\Delta E / k_B T)} \quad (4)$$

where k_B is Boltzmann's constant ($k_B = 1.380 \times 10^{-23}$ $J \cdot K^{-1}$) and T is temperature in K. A general description the Monte Carlo method can be found on Myers (1998). The excess enthalpy of mixing (ΔH_{excess}) of As solution into marcasite and pyrite series was calculated using a Monte Carlo simulation code developed by the authors at the University of Michigan. $8 \times 8 \times 8$ and $8 \times 8 \times 4$ supercells were constructed with a total of 2048 exchangeable anions for marcasite and pyrite, respectively, with edges parallel to the [100], [010] and [001] directions. The total number of "accepted" swaps in the Monte Carlo simulation over which the enthalpies are averaged was 100,000, over a total of 1,000,000 overall swaps per composition and temperature. The excess entropy and free energy of mixing (ΔS_{excess}, ΔG_{excess}, respectively) were calculated using the Bogoliubov integration scheme (Yeomans, 1992; Myers, 1998).

Finally, the long-range order parameter was calculated with respect to the most energetically favorable configuration (arsenopyrite and ordered $FeAsS_{pyr}$) in order to quantify the role of ordering for different temperatures and compositions. According to Eq. (5), $q = 1$ (highest ordering) when the number of ordered (reference) configurations in a Monte Carlo run $(As–S)_{MC}$ equals the number of ordered configurations in the reference structure ($As–S_{ref}$, e.g. ordered arsenopyrite). On the other hand, the maximum disorder with respect to the reference structure occurs when $q = 0$.

$$q = \frac{\sum (As - S)_{MC}}{\sum (As - S)_{ref}}. \quad (5)$$

3. Results

3.1. Enthalpy of mixing

The excess enthalpies of mixing (ΔH_{excess}) of As in marcasite and pyrite solid solution are presented in Fig. 3, as a function of composition X_{As} (molar fraction of As/(As+S)) and temperature T. The data, calculated from Monte Carlo runs, show that for the marcasite series, the disordered solid solution orders towards intermediate member arsenopyrite (FeAsS) at 1:1

Table 2
Exchange parameters considered to describe the enthalpy of mixing and energetics of anion ordering, for marcasite and pyrite structural series (n.n.: nearest-neighbors)

Exchange parameters J_i (eV)						
	J_1 (n.n.)	J_3 (3rd n.n.)	J_4 (4th n.n.)	J_5 (5th n.n.)	J_6 (6th n.n.)	r-square
Marcasite series	−0.27909	0.019304	−0.11998	−0.077452	3.791×10^{-12}	0.9566
Pyrite series	−0.27008	0.029338	−0.39866	0.003444	0.00000	0.9091

Composition-dependent terms E_{XAs} (eV)									
X_{As}	E_0	E_1	E_2	E_3	E_4	E_5	E_6	E_7	E_8
	0	0.125	0.25	0.375	0.5	0.675	0.75	0.875	1
Marcasite series	0.00	5.59	8.32	9.86	4.14	6.50	9.80	6.55	0.00
Pyrite series	−4.35	11.48	19.13	26.32	29.97	37.50	36.91	42.07	49.14

Goodness of fit of the Hamiltonian in Eq. (3) is presented as the r-square value (r^2). Composition-dependent terms E_{XAs} in Eq. (3) are also presented for each composition (X_{As}). Exchange parameters J_i (eV).

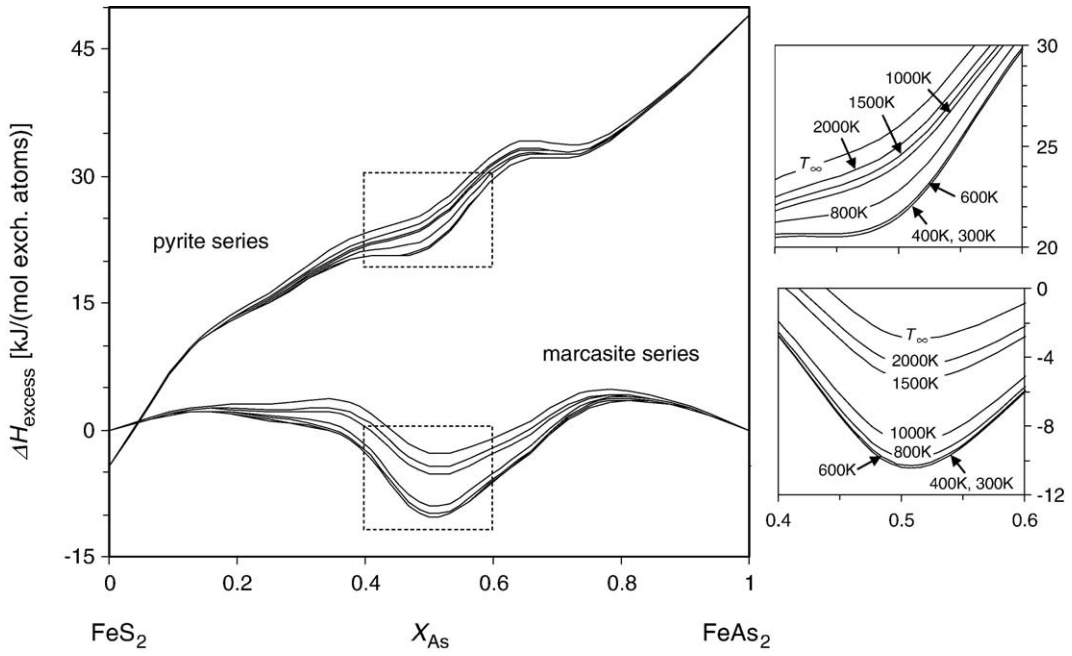

Fig. 3. Calculated excess enthalpy of mixing (ΔH_{excess}) for marcasite and pyrite solid solution series, as a function of temperature (in K) and composition (X_{As}, molar fraction of As/(As+S)). Insets detail the enthalpy curves for each temperature for the marcasite and pyrite series.

As:S ratio, expressed by a minimum at $X_{As}=0.5$, for the entire temperature range (300 K$<T<T_8$). At room temperature ($T=300$ K), arsenopyrite is ~10.5 kJ/(mol exchangeable anions) more energetically favorable than the average of the two end-members marcasite and löllingite (see inset Fig. 3).

In contrast, the pyrite solid solution series shows a different picture than marcasite, with pure pyrite end-member being ~53 kJ/(mol exchangeable anions) more energetically favorable than the virtual end-member $FeAs_2$ with pyrite structure. An important feature of Fig. 3 is the intersection of enthalpy curves at $X_{As}=0.05$, indicating that the arsenian pyrite solid solution is energetically favored by ~4 kJ/(mol exchangeable anions) with respect to the arsenian marcasite solid solution, for $X_{As}<\sim0.05$.

3.2. Gibbs free energy of mixing

Fig. 4 shows the excess Gibbs free energy of mixing (ΔG_{excess}) for the marcasite and pyrite solid solution series, calculated using a post-Monte Carlo Bogoliubov integration scheme. The data predict, for the marcasite series, nearly complete immiscibility between marcasite and arsenopyrite for temperatures below ~1000 K, as shown in Fig. 5. Limited solid solution of As in marcasite was found only below the dilute limit of $\sim X_{As}<0.05$, where the mixture of marcasite+arsenopyrite is less energetically favorable. A second miscibility gap is observed for compositions $X_{As}>\sim0.6$ where the mixture of arsenopyrite+löllingite is more stable than excess solution of As in arsenopyrite. A similar picture is predicted for the pyrite solid solution series, where nearly complete immiscibility is observed between pyrite and $FeAsS_{pyr}$ (pyrite structure FeAsS). Arsenian pyrite solid solution $Fe(S,As)_2$ is predicted to be energetically favored over FeS_2–$FeAsS_{pyr}$ two-phase mixture only for $X_{As}<0.05$.

The calculated ΔG_{excess} curves show that the equilibration of As-bearing phases is strongly favored for the marcasite series with respect of the pyrite series, although at low As compositions ($\sim X_{As}<0.05$), the solid solution of As in marcasite is energetically unfavorable with respect to As solution in pyrite. From the free energy curves in Figs. 4 and 5, a phase diagram can be constructed for the solid solution of As into iron disulfides (Fig. 6). Two miscibility gaps are predicted, where the mixtures (pyrite, marcasite)+arsenopyrite and löllingite+arsenopyrite are favored with respect to the solid solution of As in pyrite or marcasite and S in löllingite, respectively.

3.3. Configurational entropy and ordering

The configurational entropy of mixing (ΔS_{excess}) for marcasite and pyrite solid solution series was obtained

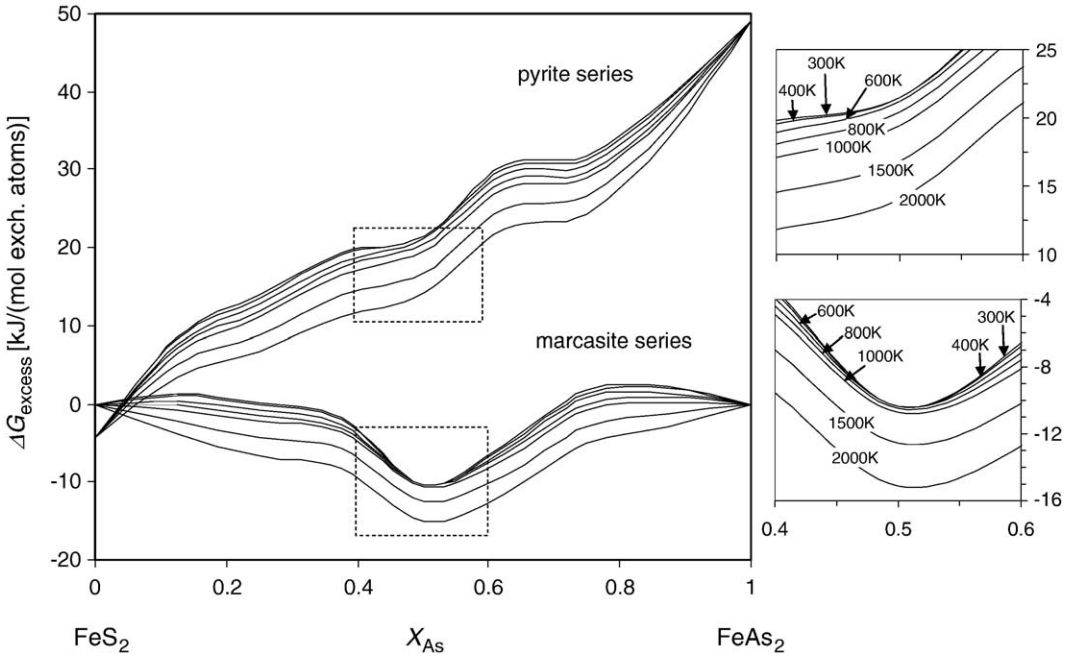

Fig. 4. Excess Gibbs free energy of mixing (ΔG_{excess}) for marcasite and pyrite solid solution series as calculated as a function of temperature (in K) and composition (X_{As}). Insets detail the free energy curves at each temperature. Miscibility gaps are predicted for both solid solution series.

from the difference between the enthalpy (from Monte Carlo runs) and the free energy of mixing (calculated using the Bogoliubov integration scheme). Fig. 7 (a) and (b) show that ordering significantly lowers the configurational entropy of both solid solution series, for intermediate compositions (X_{As} ~0.5). A significant decrease in calculated ΔS_{excess} occurs for $T<1500$ K (for the marcasite series) and $T<800$ K (for the pyrite

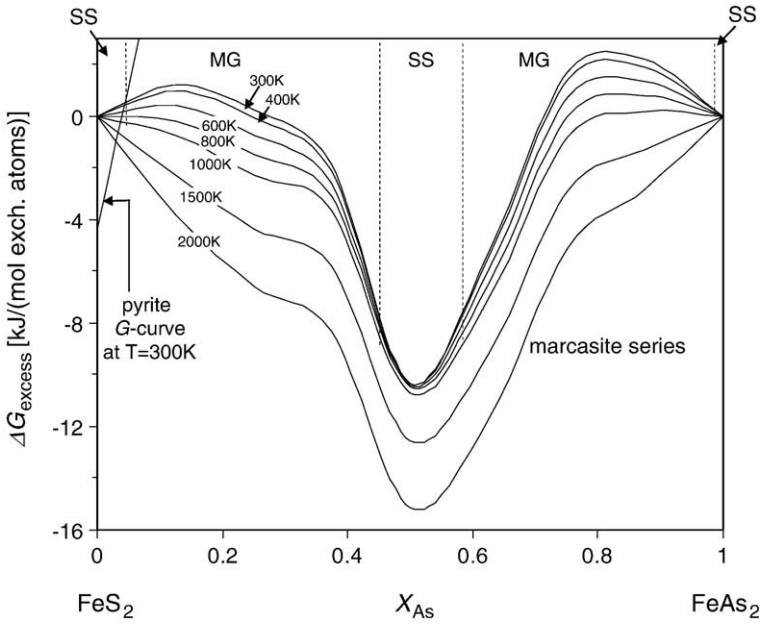

Fig. 5. Detail of the Gibbs free energy plot in Fig. 4, for the marcasite series. The oblique solid line in the upper left corner is the free energy curve of arsenian pyrite at 300 K. Vertical segmented lines separate miscibility gaps (MG) from solid solution (SS) fields. For $X_{As}<$~0.05 (~6 wt.% As), the solution of As into marcasite and pyrite is favored.

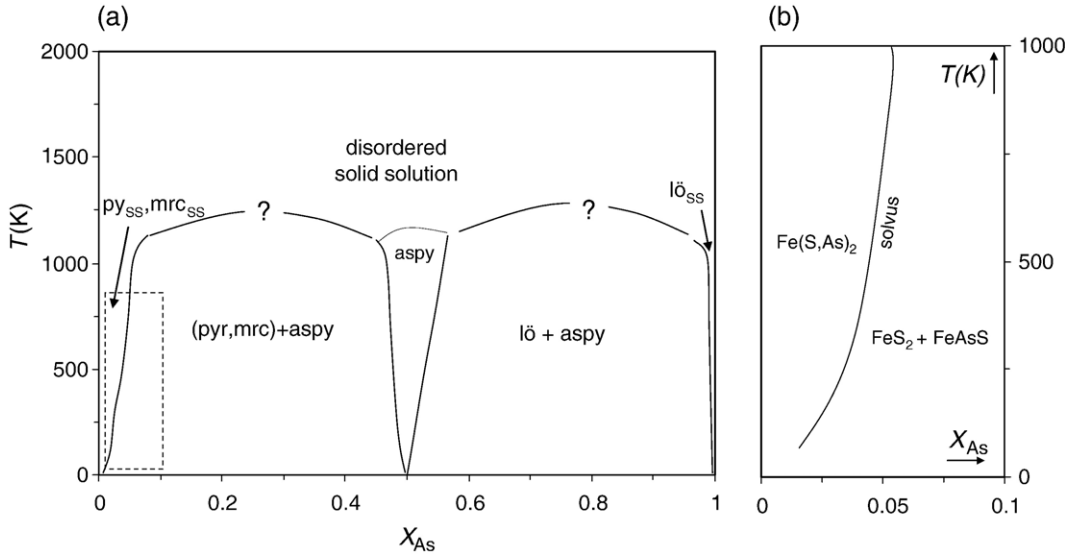

Fig. 6. (a) Calculated phase diagram for the $FeAs_2$–FeAsS–$FeAs_2$ solid solution. Note the presence of two miscibility gaps, where two phases are stable instead of a solid solution (abbreviations: py = pyrite, mrc = marcasite, aspy = arsenopyrite and lö = löllingite). The dashed region in (a) is shown in detail in (b), where $Fe(S,As)_2$ unmixes into FeS_2+FeAsS. For compositions $X_{As}<0.05$, calculations show that solid solution of As into pyrite is more energetically favorable than into marcasite.

series). Above these temperatures, ΔS_{excess} values remain only within 10% of the value of configurational entropy at infinite temperature T_∞ (point entropy, $\Delta S_{point} = -R[X_{As}\ln X_{As} + (1-X_{As})\ln(1-X_{As})] = -5.76$ J/(K·mol exchangeable anions), for $X_{As}=0.5$). The same ordering trend is observed in Fig. 8, which shows the long-range order parameter q as a function of temperature and composition ($X_{As}=0.5$). The order parameter reaches unity for $T<1500$ K (marcasite series) and $T<800$ K (pyrite series), reflecting ordering toward the intermediate members arsenopyrite (FeAsS) and ordered $FeAsS_{pyr}$ (pyrite structure FeAsS), respectively.

4. Discussion

4.1. Solid solution of As into marcasite and pyrite

Quantum-mechanical and Monte Carlo simulations results presented in the previous sections reveal important constraints on the atomic incorporation of As into pyrite and marcasite, as well as their resulting thermodynamic mixing properties. The exchange parameters J for marcasite and pyrite series are presented in Table 2 and indicate that As and S strongly interact at the atomic scale. Their magnitude and sign show that ordering in both marcasite and pyrite solid solutions promotes heteroanionic As–S nearest-neighbor and 4th-nearest neighbor interactions (negative Js). Since there is always an equal number of nearest and second nearest neighbor As–S interactions in arsenian pyrites and marcasites, promotion of As–S nearest neighbor interactions automatically means promotion of second nearest As–S neighbor interactions. Ordered arsenopyrite is the best example for this statement where *all* anionic dimer interactions are As–S interactions, and also all anionic neighbors of an anion from different dimer are As–S interactions. Homoanionic (As–As, S–S) interactions (positive Js) are promoted for 3rd nearest-neighbor interactions in both systems. In the 5th nearest neighbor range, marcasite and pyrite series show heteroanionic and homoanionic interactions, respectively. 6th nearest neighbor interactions are negligible.

The nature of As–S interactions in marcasite and pyrite result in strong non-ideal mixing behavior of the solid solution, as indicated by the non-zero excess enthalpies of mixing (ΔH_{excess}) depicted in Fig. 3. For the marcasite–löllingite series, there is a significant minimum in the enthalpy and free energy of mixing at 1:1 compositions, reflecting the ordering tendency toward thermodynamically stable arsenopyrite (Figs. 3 and 4). This behavior has been observed previously in other solid solution systems, and the best-known example is dolomite ($CaMg(CO_3)_2$), which forms an ordered compound at 1:1 compositions in the calcite ($CaCO_3$)–magnesite ($MgCO_3$) system (Burton and Kikuchi, 1984). The formation of the stable phase arsenopyrite is also reflected by the configurational entropy data in

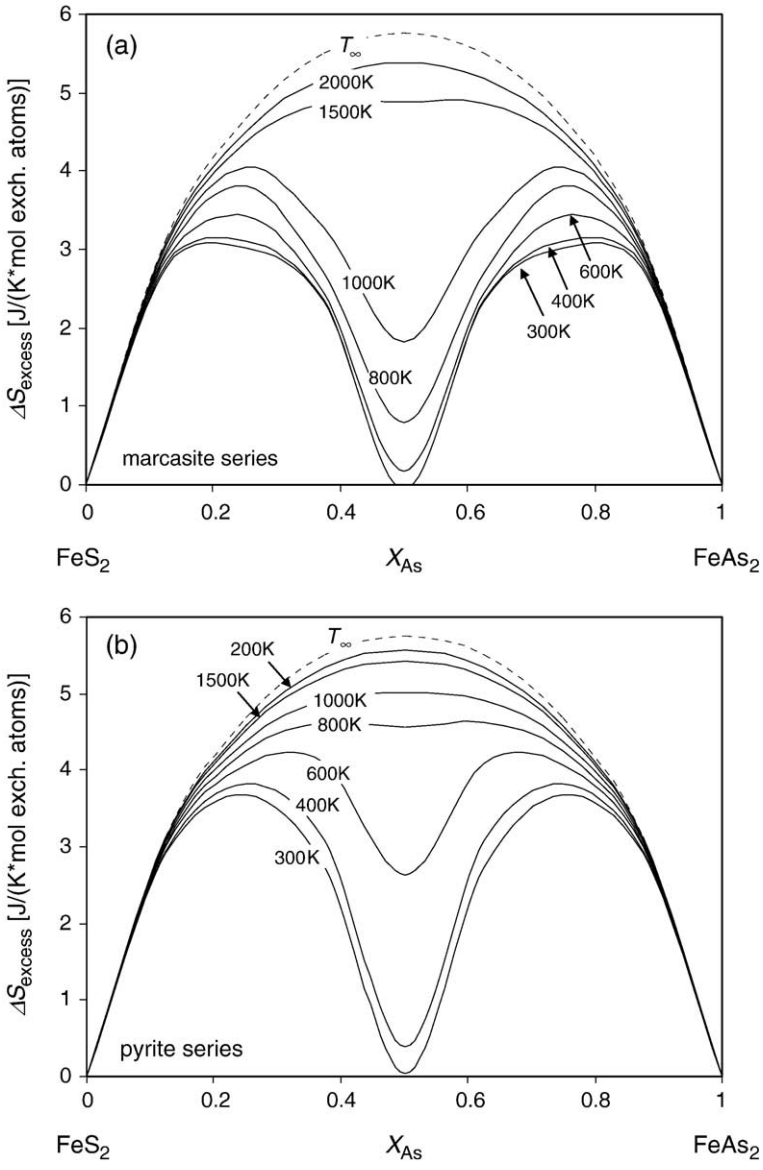

Fig. 7. Configurational excess entropy of mixing (ΔS_{excess}) calculated for marcasite (a) and pyrite (b) solid solution series, as a function of temperature and composition (X_{As}). Significant ordering is observed at $X_{As}=0.5$ for marcasite and pyrite series for equilibration temperatures below ~1500 and 800 K, respectively.

Fig. 7a, as curves dip significantly for $T<1500$ K. This ordering tendency at 1 : 1 compositions is quantified by the interaction parameter q in Fig. 8, which rapidly increases from ~0.1 to ~0.8 between 1500 and 1000 K. Below 1000 K, q approaches unity as arsenopyrite orders completely at room temperature.

According to the calculated Gibbs free energy data, arsenopyrite is predicted to be ~10 kJ/(mol exchangeable anions) more energetically favorable than the average of the two end-members marcasite and löllingite at 300 K (room temperature) (Fig. 4, inset). This theoretical value can be compared with experimental Gibbs free energy data calculated from the difference between the free energy of formation of arsenopyrite [$\Delta_f G^0_{298}=141.6\pm6$ kJ/mol, Pokrovski et al., 2002] and the average of free energies of formation for marcasite and löllingite [$\Delta_f G^0_{298}=-158.4$ kJ/mol (marcasite); $\Delta_f G^0_{298}=-52.3$ kJ/mol (löllingite), Robie and Hemingway, 1995], per mole of exchangeable anions, at 1 bar and room temperature. Arsenopyrite Gibbs free energy, when calculated from experimental data, is ~18 kJ/(mol exchangeable anions) more energetically favor-

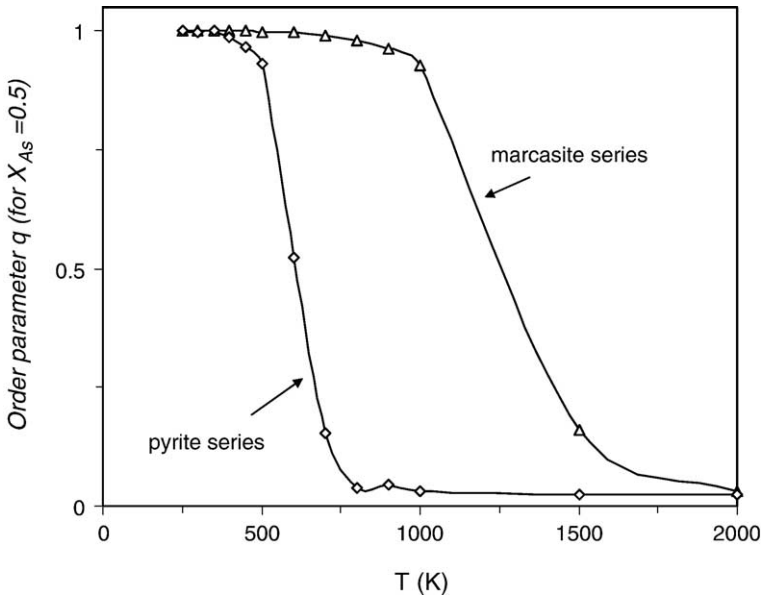

Fig. 8. Long range order parameter q as a function of T (K), for a composition $X_{As}=0.5$. Ordering occurs at $T<1500$ K and $T<800$ K for marcasite and pyrite series, respectively.

able than the average of marcasite and löllingite. Thus, our predicted value underestimates the experimental Gibbs free energy of formation for arsenopyrite by about 8 kJ/(mol exchangeable anions) (if using average value of $\Delta_f G^0_{298}=-141.6$ kJ/mol for arsenopyrite). The resulting difference between the calculated and experimental free energies is strongly dependent on the calorimetric data, and their associated errors. When incorporating the ± 6 kJ/mol deviation from average $\Delta_f G^0_{298}$ of arsenopyrite (-135.6 and -147.6 kJ/mol), the difference between predicted and experimental free energy varies from ~5 to 10 kJ/(mol exchangeable anions), respectively.

The calculated Gibbs free energy data presented in Fig. 4 predicts that, for almost all the range of As compositions ($X_{As}>0.05$), the marcasite solid solution series is energetically favored with respect to pyrite solid solution series. However, at low As concentrations ($X_{As}<0.05$), solid solution of As in pyrite is predicted to be favored over the solution of As in marcasite. Notwithstanding that the formation of pyrite versus marcasite is dependent on solution properties and reaction paths (Schoonen and Barnes, 1991a), our calculated results suggest that the pyrite structure is more prone to incorporate As at low concentrations (Figs. 3,4).

Free energy data for pyrite series also indicate the formation of intermediate-composition members that are less energetically favorable than end-member pyrite (Fig. 3,4) but more energetically favorable than $FeAs_{2pyr}$ end-member. The ordering tendency towards 1:1 compositions is inferred from configurational entropy data in Fig. 7b and the order parameter q in Fig. 8. The transition from the disordered state toward an ordered FeAsS compound with pyrite structure occurs in a narrow range of temperatures between 750 and 500 K, where q increases from ~0.05 up to unity.

4.2. Miscibility gaps and exsolution

Two miscibility gaps are observed in the phase diagram in Fig. 6. For most of the compositional range of As, a mixture of two phases is more stable than the solid solution of As into pyrite or marcasite. For example, for bulk As compositions of 25% ($X_{As}=0.25$), the mixture of $FeS_2+FeAsS$ is more stable than the solid solution of As in marcasite or pyrite, $Fe(S,As)_2$. In contrast, a mixture of $FeAsS+FeAs_2$ will dominate on the high-level portion of the As spectrum of composition. However, calculations predict that the solid solution of As into marcasite and pyrite is favorable at low As concentrations, for $X_{As}<0.05$ (~6 wt.% As). According to these results, marcasite and pyrite can eventually incorporate up to ~6 wt.% As in their structures as solid solution, without undergoing major phase transformation. For As bulk contents higher than this limit, the solid solution will become metastable, and As-rich marcasite and pyrite will eventually undergo exsolution into more stable, two-phase mixtures.

In order to evaluate exsolution, Monte Carlo simulations of ordering were performed at different As compositions for 'metastable' As-rich marcasite and pyrite, with As contents exceeding the predicted limit for solution (X_{As} ~0.05). Fig. 9 presents ball-and-stick models of the annealing process for composition X_{As}=0.25, in the center of the miscibility gap in Fig. 6a. Ordered arsenopyrite and cubic FeAsS structures, equilibrated at 300 K and X_{As}=0.5, are presented as a reference. Results of the annealing process show that when the temperature is decreased below 1500 K, disordered As atoms in marcasite tend to cluster (e.g., for T=800 K) until they form, at lower temperature (e.g. 300 K), domains of ordered arsenopyrite ||(001). For marcasite, clustering of As atoms and arsenopyrite domain formation starts at T ~1000 K. Results for 'metastable' As-rich pyrite are similar, showing that clustering of As atoms and formation of domains of $FeAsS_{pyr}$ phase, although this process starts to take place at lower temperatures (T<800 K). Although not shown here, similar exsolution processes in As-rich pyrite and marcasite is observed at lower (e.g., 12.5%) and higher (e.g., 37.5%) arsenic compositions. Therefore, the formation of domains of FeAsS is predicted to be favorable in the marcasite and pyrite series, within the miscibility gap. However, Monte Carlo simulations of the type presented in this study may overestimate the formation of nanodomains by underestimating the interface energy between the ordered arsenian sulfide domain and the host sulfide.

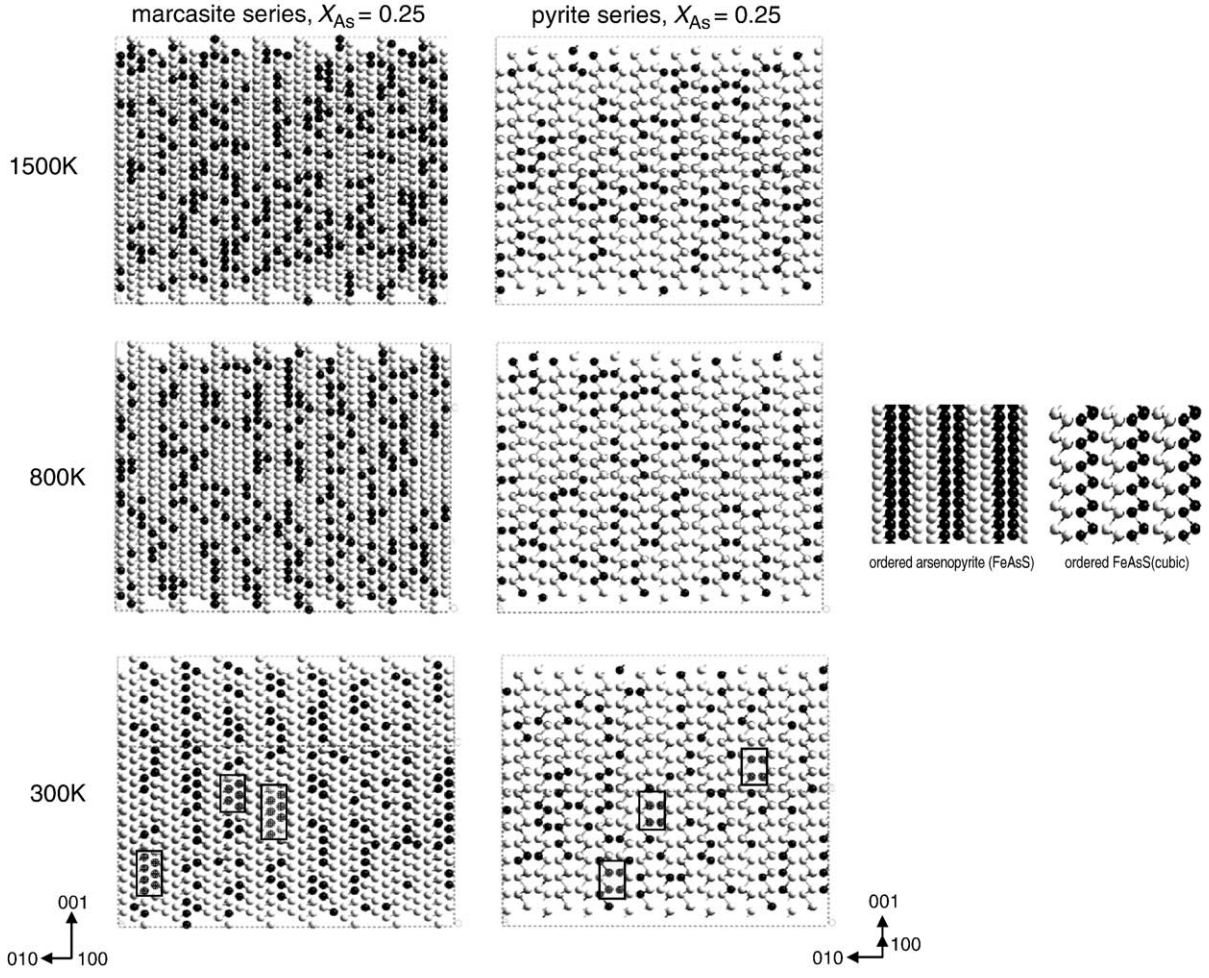

Fig. 9. Ball-and-stick models of 8 × 8 × 8 and 8 × 8 × 4 'arsenian' marcasite and pyrite supercells (X_{As}=0.25) that were most energetically favorable during Monte Carlo simulations, shown for selected temperatures (1500, 800 and 300 K). Only As (black) and S (light grey) atoms are shown. Clustering of As atoms (black balls) in both series promotes the formation of ordered FeAsS domains in both solid solution series, when temperature is decreased. Arsenopyrite (FeAsS) and cubic-FeAsS ordered structures, equilibrated at 300 K at X_{As}=0.5, are presented in the bottom as a reference. Shaded boxes indicate FeAsS nanodomain formation within FeS_2, as a result of unmixing of unstable $Fe(S,As)_2$.

4.3. Comparison with TEM studies

Although the microstructure of As-rich pyrite/marcasite is still not fully understood, a number of previously published transmission electron microscopy (TEM) studies document the nature of As-rich pyrite at the nanoscale. High-resolution TEM observations of auriferous As-rich (~8 wt.% As) arsenian pyrite from ore deposits by Fleet et al. (1989) and Simon et al. (1999a,b) suggested the presence of stacking faults separating alternating pyrite and arsenopyrite (or marcasite) structure thin (10–12 Å) lamellae. In addition, Palenik et al. (2004) documented a complex, heterogeneous matrix for auriferous arsenian pyrite (~9 wt.% As) in samples from a Carlin-type gold deposit in Nevada. The heterogeneous nature of the matrix in these samples was described as a polycrystalline mixture of pyrite and arsenopyrite (or possibly pyrrhotite) nanodomains of ~20 nm^2 in size, surrounding Au nanoparticles. These TEM observations suggest that high As-contents (e.g., >8 wt.% As) in arsenian pyrite might be related to the presence of nanoscale aggregates of sulfides, with As residing in arsenopyrite domains. In contrast, HRTEM and XAS data from Savage et al. (2000) on arsenian pyrites with lower As concentrations (~1.2 wt.% As average) from the Mother Lode District (California) suggest that As is in solid solution. HRTEM observations showed an absence of marcasite-type structure lamellae, indicative of sub-domains of arsenopyrite. Furthermore, detailed X-ray absorption spectroscopy (XAS) data (XANES, EXAFS) strongly support the substitution of As for S, where As atoms are locally clustered in the pyrite lattice, and the unit cell of arsenian pyrite is expanded in ~2.6% with respect to pure pyrite. Although arsenopyrite domains are not ruled out completely from XAS data, they were not observed in TEM images. These studies provide valuable structural and compositional information. In arsenian pyrites with As contents ~6–9 wt.% (Fleet et al., 1989; Palenik et al., 2004), arsenopyrite domains were observed in HRTEM images. In contrast, for arsenian pyrites with lower As contents (~1.2 wt.%), most of the As is in solid solution, with local clustering of As atoms. Thus, there is analytical evidence that the arsenian pyrite nanostructure is modified with increasing As contents, from As being in solid solution at low As wt.% to being unmixed into pyrite and marcasite-structure (arsenopyrite) domains.

The previous HRTEM observations support our predicted results for the solid solution of As into iron disulfides. When the calculated limit of ~6 wt.% As in pyrite is surpassed, the solid solution of As in no longer favored, and exsolution into pure pyrite and $FeAsS_{pyr}$ (cubic structure) phase occurs (Fig. 9). Although this latter phase does not occur as a mineral, the formation of pyrite-structure FeAsS domains, monolayers or lamellae may indeed occur during exsolution, although their persistence may be kinetically hindered, eventually transforming into the more energetically favorable arsenopyrite structure. Thus, the mechanism of arsenian pyrite admixture has to be investigated in detail in further studies. Furthermore, the admixture of As-rich marcasite into pure marcasite and arsenopyrite has yet to be documented and confirmed in HRTEM observation.

Therefore, the terms ‘arsenian’ pyrite and ‘arsenian’ marcasite, widely used in the literature, must be used with care as they may or may not represent a single phase at the nanoscale. According to our results, and taking into account the previously published analytical data, a distinction must be made between stable and metastable arsenian pyrite/marcasite. The former refers to a thermodynamically stable solid solution of As into pyrite and marcasite, while the latter refers to a metastable phase that eventually unmixes into polycrystalline mixture of FeS_2 + FeAsS nano-domains.

Acknowledgments

Support for this research was received from National Science Foundation Grant EAR-0309772 to U.B. Additional support was provided to M.R. through Fulbright-Mecesup and Rackham Graduate School (at U. of M.) fellowships. This research represents part of the first author’s Ph.D. dissertation at the University of Michigan, and was inspired by early work funded by National Science Foundation grant EAR-0207273 to S.E. Kesler. Finally, we acknowledge Manuel Prieto for handling the manuscript and two anonymous reviewers for their insightful comments and suggestions. **[LW]**

References

Anawar, H.M., Akai, J., Komaki, K., Terao, H., Yoshioka, T., Ishizuka, T., Safiullah, S., Kato, K., 2003. Geochemical occurrence of arsenic in groundwater of Bangladesh: sources and mobilization processes. J. Geochem. Explor. 77, 109–131.

Aylmore, M.G., 1995. Distribution and agglomeration of gold in arsenopyrite and pyrite. Unpublished Ph.D. Thesis: Curtin University of Technology, Perth, Western Australia.

Barton Jr., P.B., 1969. Thermochemical study of the system Fe–As–S. Geochim. Cosmochim. Acta 33, 841–857.

Bayliss, P., 1977. Crystal structure refinement of a weakly anisotropic pyrite. Am. Mineral. 62, 1168–1172.

Becker, U., Pollok, K., 2002. Molecular simulations of interfacial and thermodynamic mixing properties of grossular-andradite garnets. Phys. Chem. Miner. 29, 52–64.

Becker, U., Fernandez-Gonzalez, A., Prieto, M., Harrison, R., Putnis, A., 2000. Direct calculation of thermodynamic properties of the barite/celestite solid solution from molecular principles. Phys. Chem. Miner. 27, 291–300.

Bosenick, A., Dove, M.T., Geiger, C.A., 2000. Simulation studies on the pyrope–grossular garnet solid solution. Phys. Chem. Miner. 27, 398–418.

Bosenick, A., Dove, M.T., Myers, E.R., Palin, E.J., Sainz-Diaz, C.I., Guiton, B.S., Warren, M.C., Craig, M.S., Redfern, S.A.T., 2001. Computational methods for the study of energies of cation distributions; applications to cation-ordering phase transitions and solid solutions. Mineral. Mag. 65, 193–219.

Buerger, M.J., 1931. The crystal structure of marcasite. Am. Mineral. 16, 361–395.

Burton, B., Kikuchi, R., 1984. Thermodynamic analysis of the system $CaCO_3$–$MgCO_3$ in the tetrahedron approximation of the cluster variation method. Am. Mineral. 69, 165–175.

Cabri, L.J., Newville, M., Gordon, R.A., Crozier, E.D., Sutton, S.R., McManon, G., Jiang, D., 2000. Chemical speciation of gold in arsenopyrite. Can. Mineral. 38, 1265–1281.

Clark, L.A., 1960. The Fe–As–S system — phase relations and applications. Econ. Geol. 55, 1345–1381.

Cline, J.S., 2001. Timing of gold and arsenic sulfide mineral deposition at the Getchell Carlin-type gold deposit, north-central Nevada. Econ. Geol. 96, 75–89.

Dove, M.T., 2001. Computer simulations of solid solutions. EMU Notes Mineral. 3, 225–250.

Fan, A.K.L., Rosentha, Gh., Wold, A., McKinzie, H.L., 1972. Preparation and properties of $FeAs_2$ and $FeSb_2$. J. Solid State Chem. 5, 136–143.

Fleet, M.E., Mumin, A.H., 1997. Gold-bearing arsenian pyrite and marcasite and arsenopyrite from Carlin Trend gold deposits and laboratory synthesis. Am. Mineral. 82, 182–193.

Fleet, M.E., MacLean, P.J., Barbier, J., 1989. Oscillatory-zoned As-bearing pyrite from strata-bound and stratiform gold deposits; an indicator of ore fluid evolution. Econ. Geol. Monogr. 6, 356–362.

Heine, V., 1998. The role of computer experiments in mineralogy. In: Winkler B. (Eds.), 1st Kiel Workshop on the Application of Computer Simulation to Mineralogy. Berichte aus Arbeitskreisen der DGK, Kiel.

Hohenberg, P., Kohn, W., 1964. Inhomogeneous electron gas. Phys. Rev., B 136, 864–871.

Kretschmar, U., Scott, S.D., 1976. Phase relations involving arsenopyrite in the system Fe–As–S and their application. Can. Mineral. 14, 364–386.

Morimoto, N., Clark, L.A., 1961. Arsenopyrite crystal-chemical relations. Am. Mineral. 46, 1448–1469.

Myers, E.R., 1998. A statistical-mechanics model of ordering in aluminosilicate solid solutions. Phys. Chem. Miner. 25 (6), 465–468.

Palenik, C.S., Utsunomiya, S., Reich, M., Kesler, S.E., Ewing, R.C., 2004. "Invisible" gold revealed: direct imaging of gold nanoparticles in a Carlin-type deposit. Am. Mineral. 89, 1359–1366.

Payne, M.C., Teter, M.P., Allan, D.C., Arias, T.A., Joannopoulos, J.D., 1992. Iterative minimization techniques for ab initio total energy calculations: molecular dynamics and conjugate gradients. Rev. Mod. Phys. 64, 1045–1097.

Perdew, J.P., Wang, Y., 1992. Accurate and simple analytic representation of the electron-gas correlation-energy. Phys. Rev., B 45, 13244–13249.

Pokrovski, G.S., Kara, S., Roux, J., 2002. Stability and solubility of arsenopyrite, FeAsS, in crustal fluids. Geochim. Cosmochim. Acta 66, 2361–2378.

Reich, M., Palenik, C.S., Utsunomiya, S., Becker, U., Stixrude, L., Kesler, S.E., Ewing, R.C., 2003. Solubility limit of gold in arsenian pyrite from carlin-type and epithermal deposits; EMPA, SIMS, HRTEM and quantum-mechanical constraints. Geol. Soc. Am. Abstr. Progr. 35, 358.

Reich, M., Kesler, S.E., Utsunomiya, S., Palenik, C.S., Chryssoulis, S., Ewing, R.C., 2005. Solubility of gold in arsenian pyrite. Geochim. Cosmochim. Acta 69, 2781–2796.

Robie, R.A., Hemingway, B.S., 1995. Thermodynamic properties of minerals and related substances at 298.15 K and 1 bar (10^5 Pascals) pressure and at higher temperatures. U.S. Geol. Surv. Bull. Rept. B 2131 (461 pp.).

Savage, K.S., Tingle, T.N., O'Day, P.A., Waychunas, G.A., Bird, D.K., 2000. Arsenic speciation in pyrite and secondary weathering phases, Mother Lode gold district, Tuolumne County, California. Appl. Geochem. 15, 1219–1244.

Schoonen, M.A.A., Barnes, H.L., 1991a. Reactions forming pyrite and marcasite from solution: I. Nucleation of FeS_2 below 100 °C. Geochim. Cosmochim. Acta 55, 1495–1504.

Schoonen, M.A.A., Barnes, H.L., 1991b. Reactions forming pyrite and marcasite from solution: II. Via FeS precursors below 100 °C. Geochim. Cosmochim. Acta 55, 1505–1514.

Schoonen, M.A.A., Barnes, H.L., 1991c. Mechanisms of pyrite and marcasite formation from solution: III. Hydrothermal processes. Geochim. Cosmochim. Acta 55, 3491–3504.

Segall, M.D., Lindan, P.J.D., Probert, M.J., Pickard, C.J., Hasnip, P.J., Clark, S.J., Payne, M.C., 2002. First-principles simulation: ideas, illustrations and the CASTEP code. J. Phys., Condens. Matter 14, 2717–2743.

Sha, P., 1993. Geochemistry and genesis of sediment-hosted disseminated gold mineralization at the Gold Quarry mine, Nevada. Ph.D. Thesis, University of Alabama, Tuscaloosa.

Sidle, W.C., Wotten, B., Murphy, E., 2001. Provenance of geogenic arsenic in the Goose River basin, Maine, USA. Environ. Geol. 41, 62–73.

Simon, G., Huang, H., Penner-Hahn, J.E., Kesler, S.E., Kao, L.-S., 1999a. Oxidation state of gold and arsenic in gold-bearing arsenian pyrite. Am. Mineral. 84, 1071–1079.

Simon, G., Kesler, S.E., Chryssoulis, S., 1999b. Geochemistry and textures of gold-bearing arsenian pyrite, Twin Creeks, Nevada; implications for deposition of gold in Carlin-type deposits. Econ. Geol. 94, 405–421.

Utsunomiya, S., Peters, S.C., Blum, J.D., Ewing, R.C., 2003. Nanoscale mineralogy of arsenic in a region of New Hampshire with elevated As-concentrations in the groundwater. Am. Mineral. 88, 1844–1852.

Vanderbilt, D., 1990. Soft self-consistent pseudopotentials in a generalized eigenvalue formalism. Phys. Rev., B 41, 7892–7895.

Yeomans, J.M., 1992. Statistical Mechanics of Phase Transitions. Oxford Science Publications, Clarendon Press, Oxford. 168 pp.